X–Ray Properties of the GigaHertz–Peaked and Compact Steep Spectrum Sources

Stephanie LaMassa[1], A. Siemiginowska[1], T. L. Aldcroft[1], M. Guianazzi[2], J. Bechtold[3], M. Elvis[1]

[1] Harvard–Smithsonian Center for Astrophysics
[2] European Space Astronomy Center of ESA
[3] Steward Observatory, University of Arizona

Introduction

• Giga-Hertz Peaked Spectrum (GPS) sources have compact radio morphology peaking at 1 GHz in the radio spectrum.
• We present the *Chandra* observations and analysis of a sample of 17 GPS sources: 14 quasars and 3 galaxies.
• The GPS galaxies are highly luminous ($> 10^{45}$ erg/sec) and show little intrinsic galactic absorption.

Analysis

• All sources were observed with *Chandra*, using ACIS-S.
• The data were processed with CIAO 3.2 and CALDB 3.0 calibration files.
• Figure 1 is a histogram of number of sources versus redshift.

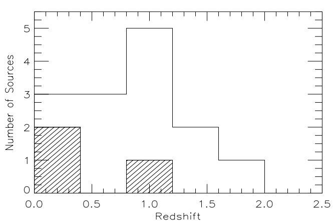

Figure 1: Histogram of number of sources vs. redshift. Galaxies denoted by filled regions; empty regions are quasars.

Image Analysis

• Figure 2 shows the raw *Chandra* ACIS-S images of several sources which have extended X-ray emissions: Q0740+380, Q1250+568, Q1328+254, and PKS B1345+125.
• An X-ray image of PKS 1345+125 with X-ray contours overlaid is shown in Figure 3. The X-ray data were smoothed using a Gaussian function.
• Figure 4 depicts an adaptively smoothed X-ray image of Q0740+380 in both the soft band (0.5-2 keV) and the hard band (2-7 keV).

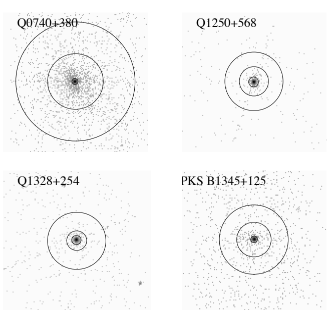

Figure 2: Raw *Chandra* ACIS–S images of 4 GPS/CSS sources that have extended X–Ray emission. The pixel size is the standard ACIS pixel of 0.492 arcseconds.

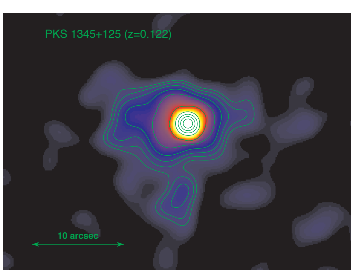

Figure 3: Smoothed X–ray image of PKS B1345+125 with X–ray contours overlaid. [Siemiginowska et al. (2005)] The X–ray extension corresponds to the VLBI jet propogating in the South–West direction [Stanghellini et al. (2001)].

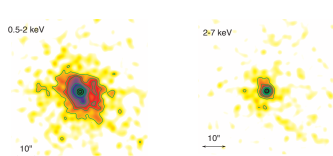

Figure 4: Adaptively smoothed image of Q0740+380 in two x–ray bands: soft 0.5–2 keV on the left and hard 2–7 keV on the right. Contours represent a surface brightness of (0.036, 0.066, 0.11, 0.3, 0.66, 6.635, 33.175) x 10^{-6}photons cm^{-2}arcsec^{-2}. 1" = 8.2 kpc [Siemiginowska et al. (2005, ApJ)]

Abstract

Giga-Hertz Peaked Spectrum (GPS) radio sources are powerful radio and X-rays emitters. Their radio properties have been extensively studied leading to two possible explanations of the compact nature of the GPS sources: (1) *frustrated source* scenario in which the expansion of the radio source is confined by a dense environment; (2) *evolution scenario* in which the source is at an early stage of its expansion to a typical large scale radio source. Measurements of the expansion velocity of the radio components in several GPS sources (Compact Symmetric Objects) suggest that these sources are young, while there has been no evidence for a dense medium required for the source confinement. Here we consider a sample GPS sources, containing both galaxies and quasars, observed with *Chandra* and *XMM-Newton*. *Chandra* observations allow for detailed studies of the source morphology on arcsec scale and we discuss different type of observed X-ray morphology for our sample. Spectral modeling of *Chandra* and XMM-*Newton* data indicate that the GPS galaxies are more obscured than quasars. We discuss the implication of this finding on our understanding of the nature of GPS sources.

Spectral Analysis

• The spectra were fit with an absorbed power law model in *Sherpa*
$N(E) = AE^{-\Gamma} * \exp^{-N_H^{gal}\sigma(E) - N_H^{abs}\sigma(E(1+z_{abs}))}$ photons cm^{-2} sec^{-1} keV^{-1}
  • A is the normalization at 1 keV
  • Γ is the photon index of the power law.
• We assumed two components for the absorption:
  • Galactic absorption due to the equivalent neutral Hydrogen column.
  • Absorption intrinsic to the quasar.
• Results of the fit are presented in Table 1.
• Three sources with non-negligible pileup were fit with JDPILEUP in *Sherpa*. Results of this fit are shown in Table 2.
• Histograms for the number of sources versus absorption are shown in Figure 5; GPS galaxies, including sources from Guainazzi et al. (2005), are represented in the plot on the left and GPS quasars are depicted in the plot on the right.
• Figure 6 is a plot of the ratio of the X-ray luminosity to the radio luminosity (at 5GHz from Stanghellini et al, 1998 and O'Dea, 1998) against redshift. The typical values for blazars, radio loud quasars, and FRI regions are demarcated on the plot.

Table 1: Absorbed Power Law Model Fits.

	gal nH 10^{20}	abs nH 10^{20}	abs Redshift	Γ	Norm [1 keV] 10^{-5}ph/cm^2/s	Flux [2-10keV] 10^{-13}erg/cm^2/s	L_x [2-10keV] 10^{44}erg/s	χ^2 (DOF)
Q0740+380	5.6	<5.06	1.063	$2.04^{+0.06}_{-0.06}$	$7.61^{+0.30}_{-0.29}$	1.84	5.43	104.5(78)
Q1143-245	5.2	<98.1	1.950	$1.69^{+0.28}_{-0.18}$	$6.01^{+1.27}_{-0.77}$	2.48	23.25	22.6(11)
Q1250+568	1.2	<0.75	0.320	$1.86^{+0.05}_{-0.05}$	$21.98^{+0.69}_{-0.71}$	7.02	1.75	90.3(74)
Q1328+254	1.1	<6.75	1.055	$1.83^{+0.06}_{-0.06}$	$12.23^{+0.53}_{-0.50}$	4.08	11.88	96.9(75)
Q0615+820	5.3	<1.88	0.770	$1.73^{+0.05}_{-0.05}$	$6.39^{+0.22}_{-0.23}$	2.46	3.81	101.4(83)
Q1458+718	2.3	<0.94	0.905	$1.56^{+0.03}_{-0.03}$	$37.17^{+0.85}_{-0.87}$	19.00	40.74	120.1(82)
B2 0738+313	4.2	$9.1^{+3.4}_{-3.2}$	0.630	$1.45^{+0.06}_{-0.06}$	$15.09^{+0.82}_{-0.78}$	4.74	4.84	154.0(84)
Q1127-145	4.1	$27.1^{+3.5}_{-3.4}$	1.180	$1.18^{+0.03}_{-0.03}$	$58.18^{+1.52}_{-1.48}$	29.53	107.28	174.3(84)
PKS B1345+125[G]	1.9	$273.8^{+88.7}_{-78.3}$	0.122	$1.15^{+0.38}_{-0.36}$	$14.22^{+11.12}_{-6.05}$			92.2(74)
Targets below did not have enough counts to fit abs nH and gamma indepedently.								
Q1829+290	11.2			$1.83^{+0.64}_{-0.60}$	$0.57^{+0.27}_{-0.20}$	0.19	0.33	158.8(1)
PKS B2128+048[G]	5.2			$1.22^{+0.36}_{-0.37}$	$1.82^{+0.37}_{-0.38}$	1.62	4.15	1.2(3)
Q1245-197	4.7			$2.01^{+0.37}_{-0.36}$	$1.26^{+0.31}_{-0.27}$	0.32	1.29	348.1(1)
Q1815+614	3.9			$1.78^{+0.26}_{-0.25}$	$4.03^{+0.54}_{-0.55}$	1.45	1.35	7.9(7)
PKS B0941-080[G]	3.7			$2.79^{+0.98}_{-0.90}$	$0.22^{+0.15}_{-0.11}$	0.02	0.003	164.4(1)
Targets below had count pile-up.								
Q1231+481	1.2	<2.63	0.375	$1.76^{+0.11}_{-0.10}$	$14.38^{+0.96}_{-0.97}$	5.30	1.84	32.4(32)
Q0134+329	4.5	<0.19	0.367	$2.24^{+0.04}_{-0.04}$	$91.78^{+1.89}_{-1.94}$	16.48	5.47	239.7(75)
Q1416+067	2.2	$14.3^{+4.1}_{-3.9}$	1.439	$1.75^{+0.04}_{-0.04}$	$71.57^{+2.01}_{-1.94}$	18.45	98.36	110.7(81)

[G]Galaxy

Table 2: Pile–up Fits

	Γ with *jdpileup*	Γ without *jdpileup*	Pileup Fraction[a]	Pileup Estimate[b]
Q1231+481	$2.26^{+0.20}_{-0.16}$	$1.76^{+0.11}_{-0.10}$	0.25	0.15
Q0134+329	$2.58^{+0.08}_{-0.08}$	$2.24^{+0.04}_{-0.04}$	0.22	0.10
Q1416+067	$1.93^{+0.05}_{-0.05}$	$1.75^{+0.04}_{-0.04}$	0.10	0.08

Q1416+067 included abs.nH in the pile-up fit since it was detected in the previous fit. Q1231+481 and Q0134+329 did not include this absorption parameter for the pile-up fit since only an upper limit was found.
[a] From *Sherpa*
[b] From the POG

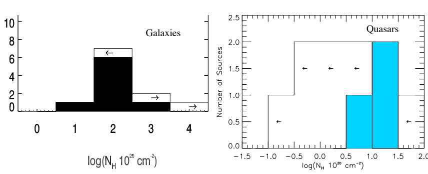

Figure 5: Histogram of number of sources vs. absorption. Plot on the left is for GPS galaxies [Guainazzi et al (2005)] and plot on the right represents GPS quasars. Absorption detection is indicated by the filled regions and upper and lower limits are denoted by the left–facing and right–facing arrows, respectively.

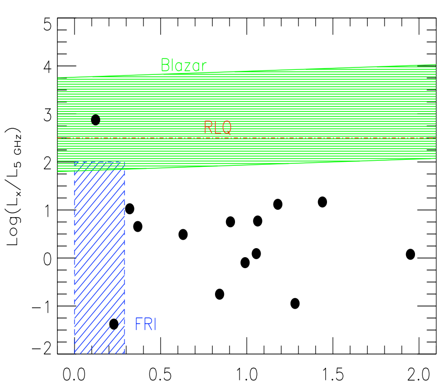

Figure 6: Ratio of X–ray luminosity to radio luminosity at 5GHz vs. redshift. The standard ranges for FRI sources, radio loud quasars and blazars [Guinazzi et al, 2005] are indicated.

Spectral Energy Distributions (SEDs)

• Photometric data points for the sources were downloaded from the NASA/IPAC Extragalactic Database (NED).
• These points, as well as the X-Ray flux at 1 keV calculated through *Sherpa*, were plotted in units of νL_ν (erg/s) along with the model SED for a radio quiet quasar (Elvis, et al., 1994).
• Figure 7 shows the SEDs for 4 of the quasars in our sample: Q0134+329, Q0740+380, Q1416+067, and Q1328+254. The Elvis SED was normalized to match the data at 1 micron for these sources.
• A plot of the SED for galaxy PKS B1345+125 is depicted in Figure 8. The Elvis SED was normalized at 4.85 GHz for this source.

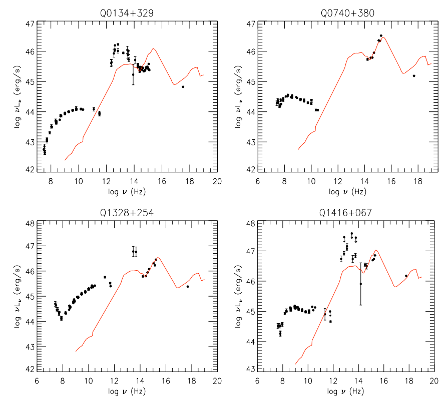

Figure 7: SED plots for a sample of quasars in our survey. Data indicated by black circles. Elvis model for a radio loud quasar denoted by red line, normalized at 1 micron. Sources (from top left to bottom right): Q0134+329, Q0740+380, Q1328+254, and Q1416+067.

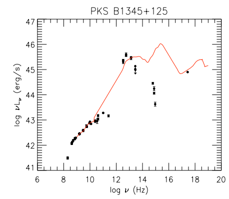

Figure 8: SED plot of GPS galaxy PKS B1345+125; data denoted by black circles and Elvis model for a radio loud quasar indicated by the red line. The model was normalized at 4.85 GHz.

Results

• The GPS galaxies in this sample were more absorbed than the quasars.
• Three out of the 17 sources exhibited significant pileup; adding the pile-up model into the analysis resulted in a steeper spectrum for these sources.
• The SEDs indicate the sources are more radio loud than the standard radio loud quasar in Elvis et al 1994 sample.

References

Elvis, Martin, Wilkes, Belinda J., McDowell, Jonathan C., Green, Richard F., Bechtold, Jill, Willner, S. P., Oey, M. S., Polomski, Elisha, & Cutri, Roc 1994, ApJS, 95, 1E
Guainazzi, Matteo, et al 2005, A&A in press (astro-ph/0509043)
O'Dea, C. P. 1998, PASP, 110, 493
Siemiginowska, Aneta, Cheung, C. C., LaMassa, Stephanie, Burke, D. J., Aldcroft, Thomas L., Bechtold, Jill, Elvis, Martin, & Worrall, D. M., 2005, ApJ, 632, 110S
Siemiginowska, A., Aldcroft, T. L., Bechtold, J., Elvis, M., & Stanghellini, C. 2005, X-Ray and Radio Connections (eds. L.O. Sjouwerman and K.K Dyer) Published electronically by NRAO, http://www.aoc.nrao.edu/events/xraydio Held 3-6 February 2004 in Santa Fe, New Mexico, USA, (E7.23) 5 pages
Stanghellini, C., Dallacasa, D., O'Dea, C. P., Baum, S. A., Fanti, R., & Fanti, C. 2001, A&A, 377, 377
Stanghellini, C., O'Dea, C. P., Dallacasa, D., Baum, S. A., Fanti, R., & Fanti, C. 1998, A&AS, 131, 303

Acknowledgements

This research is funded in part by NASA contract NAS8-39073. Partial support for this work was provided by the National Aeronautics and Space Administration through Chandra Award Number GO-01164X and GO2-3148A issued by the Chandra X-Ray Observatory Center, which is operated by the Smithsonian Astrophysical Observatory for and on behalf of NASA under contract NAS8-39073. Partial support was also provided through NASA grants NAG5-13267 NNG04GF98G.